high-power heteronuclear decoupling. Implementation of these techniques to solid-state problems is under active investigation in our laboratory.

Acknowledgment. We wish to thank Dr. Klaus Eichele for providing compounds 3 and 7 and for helpful discussions concerning this work. We are grateful to the NSERC of Canada for financial support.

OM920184T

Photoelectron Spectroscopy of f-Element Organometallic Complexes. 8.† DV-Xα and Gas-Phase UV Photoelectron Spectroscopic Investigation of the Electronic Structure of Tris(η^5-cyclopentadienyl)uranium(IV) Complexes‡

Antonino Gulino, Enrico Ciliberto, Santo Di Bella, and Ignazio Fragalà*

Dipartimento di Scienze Chimiche, Università di Catania, Viale A. Doria 6, 95125 Catania, Italy

Afif M. Seyam§ and Tobin J. Marks*

Department of Chemistry, Northwestern University, Evanston, Illinois 60208-3113

Received April 22, 1992

The electronic structures of a series of closely related $U(\eta^5\text{-}C_5H_5)_3L$ (L = $-CH_3$, $-NH_2$, $-BH_4$, -NCS) complexes has been studied using the SCF Hartree-Fock-Slater first-principles discrete variational Xα method in combination with He I and He II UV photoelectron spectroscopy. The theoretical results reproduce the experimental He I and He II photoelectron spectroscopic data, thus providing a reliable description of the metal-ligand bonding. Symmetry considerations render the 5f elements well-suited templates for coordination of the Cp_3 ligand cluster. Interactions not restricted by symmetry appear partially or entirely modulated by the angular properties of π_2-related MO's. Bonding interactions with ancillary L ligands involve either $5f_{z^3}$ or $6d_{z^2}$ metal orbitals, depending upon the energies of the unperturbed ligand orbital counterparts. Metal-ligand interactions cause the energies of 5f orbitals to split into a narrow manifold with a remarkable "ligand field" energy shift associated only with the $5f_{y(3x^2-y^2)}$ orbital. The L→M charge donation results in an electronic configuration of the uranium atom which is almost constant throughout the $U(C_5H_5)_3L$ series and similar to that found in a fully relativistic SCF Dirac-Slater calculation on the simpler uranium atom. The stringent necessity of maintaining the uranium center in a particularly stable electronic configuration causes greater donation (hence larger covalency in the bonding) from ancillary L ligands to be compensated for by an increasing (L = $-NH_2$ < $-CH_3$ < -NCS < BH_4^-) ionic character of the U-Cp bonds. The present results show that nonrelativistic DV-Xα calculations, optimized for basis set and potential representation, reproduce experimental photoelectron spectroscopic data, including He I/He II relative intensity changes.

Introduction

Actinide organometallic chemistry today represents a large and active research area.[1] Among the variety of new molecules that have been reported since the earliest synthesis of UCp_3Cl (Cp = η^5-C_5H_5),[2] Cp-actinide complexes still represent a cornerstone because of their rich chemistry and structural variety. The important problem associated with understanding actinide molecular electronic structures has, conversely, received considerable attention only recently[1,3] and, in addition to classical 5f coordination complexes,[4] a number of reports have focused on organometallic molecules, including $Cp_{4-x}AnL_x$ complexes.[3,5] Theoretical as well as experimental studies have shown that the metal-ligand bonding involves donation of ligand electron density into both metal 5f and 6d atomic orbitals.[5] Evidence has also been provided for metal→ligand back-donation for those ancillary L ligands having π-acidic character.[6] Nevertheless, details of 5f vs 6d metal contributions to the bonding still remain an open question. The variation of the He I vs He II relative photoelectron (PE) spectroscopic peak intensities[3b,7] has provided experimental evidence of metal 5f involvement because of

† Part 7: Reference 5j.

‡ Abstracted in part from the Ph.D. Thesis of A. Gulino, Università di Catania, 1989.

§ On leave from the Department of Chemistry, University of Jordan, Amman, Jordan.

(1) (a) Bursten, B. E.; Strittmatter, R. J. *Angew. Chem., Int. Ed. Engl.* **1991**, *30*, 1069-1085. (b) Marks, T. J.; Streitwieser, A., Jr. In *The Chemistry of the Actinide Elements*; Katz, J. J., Seaborg, G. T., Morss, L. R., Eds.; Chapman and Hall: London, 1986; Vol. 2, pp 1547-1587. (c) Marks, T. J. In *The Chemistry of the Actinide Elements*, 2nd ed.; Katz, J. J., Seaborg, G. T., Morss, L. R., Eds.; Chapman and Hall: London, 1986; Vol. 2, pp 1588-1627. (d) *Fundamental and Technological Aspects of Organo-f-Element Chemistry*; Marks, T. J., Fragalà, I. L., Eds.; D. Reidel: Dordrecht, Holland, 1985. (e) Marks, T. J.; Ernst, R. D. In *Comprehensive Organometallic Chemistry*; Wilkinson, G., Stone, F. G. A., Abel, E. W., Eds.; Pergamon Press: Oxford, U.K., 1982; Chapter 21, and references therein. (f) Marks, T. J. *Science* **1982**, *217*, 989 and references therein. (g) *Actinides in Perspective*; Edelstein, N. M., Ed.; Pergamon Press: Oxford, U.K., 1981. (h) Marks, T. J.; Manriquez, J. M.; Fagan, P. J.; Day, V. W.; Day, C. S.; Vollmer, S. H. *ACS Symp. Ser.* **1980**, *No. 131*, 1. (i) Marks, T. J. *Prog. Inorg. Chem.* **1979**, *25*, 224-333 and references therein. (j) *Organometallics of f-Elements*; Marks, T. J., Fischer, R. D., Eds.; D. Reidel: Dordrecht, Holland, 1979, and references therein.

(2) Reynolds, L. T.; Wilkinson, G. *J. Inorg. Nucl. Chem.* **1956**, *2*, 246-253.

(3) (a) Fischer, R. D. *Angew. Chem., Int. Ed. Engl.* **1965**, *4*, 972. (b) Fragalà, I. In ref 1j, pp 421-466. (c) Fragalà, I.; Gulino, A. In ref 1d, pp 327-360. (d) Burns, C. J.; Bursten, B. E. *Comments Inorg. Chem.* **1989**, *2*, 61-93. (e) Pepper, M.; Bursten, B. E. *Chem. Rev.* **1991**, *91*, 719-741.

(4) (a) Fragalà, I.; Condorelli, G.; Tondello, E.; Cassol, A. *Inorg. Chem.* **1978**, *17*, 3175-3179. (b) Casarin, M.; Ciliberto, E.; Fragalà, I.; Granozzi, G. *Inorg. Chim. Acta* **1982**, *64*, L247-L249. (c) Bursten, B. E.; Casarin, M.; Ellis, D. E.; Fragalà, I.; Marks, T. J. *Inorg. Chem.* **1986**, *25*, 1257-1261.

0276-7333/92/2311-3248$03.00/0

the very favorable He II/He I 5f cross-section ratio. Accurate quasi-relativistic Xα–SW calculations,[8] although they neglect relativistic effects in the critical intersphere regions of muffin-tin geometries, have indicated that the differential expansion of 5f and 6d metal wave functions causes over- and underestimation of metal 5f vs 6d metal–ligand bond covalency, respectively. The application of high-level ab initio techniques, including spin–orbit and relativistic core potentials, has revealed a major role for the metal 6d orbitals in the bonding.[9] Combined first-principles discrete variational Xα calculations also including the use of the Dirac–Slater local density operators (fully relativistic) point to a more intriguing influence of the heavy atoms. They show[10] that the relative involvement of 5f vs 6d orbitals in the metal–ligand bonding of U(IV) complexes depends upon the energy position of the particular MO being considered; that is, higher energy orbitals have significant 5f admixture whereas lower energy orbitals are dominated by 6d interactions. Analogous results were found with nonrelativistic calculations, although with some overestimation of the 5f contributions to higher energy orbitals.[8] Nevertheless, one must bear in mind that (i) even sophisticated PE measurements using synchrotron radiation have been no more informative regarding quantitative "d" vs "f" orbital admixtures and (ii) it has been shown[4c,5i] that appropriate choices of basis set and orbital representation are capable of providing accurate, computationally efficient fitting of PE data at the nonrelativistic level. Also, in this perspective, the choice must be based upon the particular observables being fitted to theoretical results, since this is the only means of calibrating their reliability.

In this context, and as a part of our ongoing studies of the electronic structure of f-metal organometallics,[3b,c,5a–c,e,h–j] we have embarked on investigations of an intriguing series of $AnCp_3L$ organometallic complexes, where the ancillary L ligand is capable of a multihapto, heavily ionic bond (L = $-BH_4$),[11] or of a nearly pure σ bond (L = $-CH_3$)[11] or possesses both σ- and π-bonding capabilities (L = $-NR_2$, –NCS, –OR)[11] while the Cp_3 ligand cluster remains fixed. We compare here results of SCF Hartree–Fock–Slater first-principles discrete variational Xα method (Xα–DVM) calculations with experimental PE data, including He I and He II intensity measurements. Fully relativistic Dirac–Slater local density calculations, to be reported in a forthcoming paper,[10c] have necessarily been limited to the series of metal alkoxides $AnCp_3OR$ (An = Ce, Th, U). Nevertheless, it must be emphasized that this comparative study shows that the overall descriptions of the metal–ligand bonding are comparable in both cases and raise significant doubt as to whether an admittedly more rigorous evaluation of 5f vs 6d admixtures is worth the prodigious computational effort needed to handle fully relativistic calculations.

Experimental Section

UCp_3L complexes (L = $-CH_3$, $-NEt_2$, $-BH_4$, and –NCS) were synthesized according to published procedures.[12] They were purified by sublimation in vacuo and always handled under prepurified argon atmospheres. They gave satisfactory analytical results. High-resolution UV photoelectron spectra were accumulated via an IBM AT computer directly interfaced to the PE spectrometer, in turn equipped with a He I, He II (Helectros-Development) source. Resolution measured on the Ar $^2P_{3/2}$ line was always ca. 20–25 meV. He II spectra were corrected only for the He IIβ "satellite" contributions (9–11% on a reference N_2 spectrum). The spectra were recorded over a wide 125–180 °C temperature range. The spectral profiles were found to be constant in that range, thus providing no evidence of any decomposition and/or ligand scrambling processes accompanying sublimation.

Computational Details

Quantum-mechanical calculations were carried out using the DV–Xα formalism.[13] The molecular electron density was approximated with an s-wave expansion to evaluate the Coulomb potential, and the SCF equations were converged by using a self-consistent charge (SCC) procedure.[13] In the case of UCp_3CH_3, the molecular potential was improved by including multipolar fitting functions, which allows a very accurate description of the charge density.[13e] Five radial degrees of freedom were allowed in the expansion of the density, in addition to the radial atomic density.[13e] Numerical AO's (atomic orbitals) (through 7p on U, 3d on S, 2p on N, C, and B, and 1s on H) were used as basis functions.[13] Several numerical calculations were carried out in order to find the best basis set.[4c,14] The integration mesh was constructed by distributing 2400 points around the uranium atom, while 300 points were generated around the S atom, 150 points around the B, C, and N atoms, and finally 75 points around the H atoms. A total of 6300–6600 sample points were used. A frozen core approximation (1s, ..., 5p on U, 1s, ..., 2p on S, and 1s on B, C, N) has been used throughout the calculations.[13] The ionization

(5) (a) Fragalà, I.; Ciliberto, E.; Fischer, R. D.; Sienel, G.; Zanella, P. *J. Organomet. Chem.* **1976**, *120*, C9–C12. (b) Fragalà, I.; Condorelli, G.; Zanella, P.; Tondello, E. *J. Organomet. Chem.* **1976**, *122*, 357–363. (c) Ciliberto, E.; Condorelli, G.; Fagan, P. J.; Manriquez, J. M.; Fragalà, I.; Marks, T. J. *J. Am. Chem. Soc.* **1981**, *103*, 4755–4759. (d) Green, J. C.; Kelly, M. R.; Long, J. A.; Kannellakopulos, B.; Yarrow, P. I. W. *J. Organomet. Chem.* **1981**, *212*, 329–340. (e) Bruno, G.; Ciliberto, E.; Fischer, R. D.; Fragalà, I.; Spiegl, A. W. *Organometallics* **1983**, *2*, 1060–1062. (f) Green, J. C.; Payne, M. P.; Streitwieser, A., Jr. *Organometallics* **1983**, *2*, 1707–1710. (g) Tatsumi, K.; Hoffmann, R. *Inorg. Chem.* **1984**, *23*, 1633–1634. (h) Bursten, B. E.; Casarin, M.; Di Bella, S.; Fang, A.; Fragalà, I. *Inorg. Chem.* **1985**, *24*, 2169–2173. (i) Vittadini, A.; Casarin, M.; Ajò, D.; Bertoncello, R.; Ciliberto, E.; Gulino, A.; Fragalà, I. *Inorg. Chim. Acta* **1986**, *121*, L23–L25. (j) Arduini, A. L.; Malito, J.; Takats, J.; Ciliberto, E.; Fragalà, I.; Zanella, P. *J. Organomet. Chem.* **1987**, *326*, 49–58.

(6) (a) Bursten, B. E.; Strittmatter, R. J. *J. Am. Chem. Soc.* **1987**, *109*, 6606–6608. (b) Brennan, J. G.; Andersen, R. A.; Robbins, J. L. *J. Am. Chem. Soc.* **1986**, *108*, 335–336. (c) Kunze, K. R.; Hauge, R. H.; Hamill, D.; Margrave, J. L. *J. Phys. Chem.* **1977**, *81*, 1664–1667. (d) Sheline, R. K.; Slater, J. L. *Angew. Chem., Int. Ed. Engl.* **1975**, *14*, 309–316. (e) Slater, J. L.; Sheline, R. K.; Lin, K. C.; Weltner, W., Jr. *J. Chem. Phys.* **1971**, *55*, 5129–5130. (f) Roberts, L. E. J. *J. Chem. Soc.* **1955**, 3939–3946.

(7) Brennan, J. G.; Green, J. C.; Redfern, C. M. *J. Am. Chem. Soc.* **1989**, *111*, 2373–2377.

(8) (a) Rösch, N.; Streitwieser, A., Jr. *J. Am. Chem. Soc.* **1983**, *105*, 7237–7240. (b) Rösch, N. *Inorg. Chim. Acta* **1984**, *94*, 297–299. (c) Höhl, D.; Rösch, N. *Inorg. Chem.* **1986**, *25*, 2711–2718. (d) Bursten, B. E.; Rhodes, L. F.; Strittmatter, R. J. *J. Am. Chem. Soc.* **1989**, *111*, 2758–2766. (e) Bursten, B. E.; Rhodes, L. F. Strittmatter, R. J. *J. Am. Chem. Soc.* **1989**, *111*, 2756–2758. (f) Strittmatter, R. J.; Bursten, B. E. *J. Am. Chem. Soc.* **1991**, *113*, 552–559.

(9) Chang, A. H. H.; Pitzer, R. M. *J. Am. Chem. Soc.* **1989**, *111*, 2500–2507.

(10) (a) Höhl, D.; Ellis, D. E.; Rösch, N. *Inorg. Chim. Acta* **1987**, *127*, 195–202. (b) Boerrigter, P. M.; Baerends, E. J.; Snijders, J. G. *Chem. Phys.* **1988**, *122*, 357–374. (c) Gulino, A.; Di Bella, S.; Fragalà, I.; Seyam, A. M.; Marks, T. J., to be submitted for publication.

(11) Fischer, R. D. In ref 1d, pp 277–326.

(12) (a) Fischer, E. O.; Hristidu. Y. *Z. Naturforsch., B* **1962**, *17*, 275. (b) Anderson, M. L.; Crisler, L. R. *J. Organomet. Chem.* **1969**, *17*, 345–348. (c) Brandi, G.; Brunelli, M.; Lugli, G.; Mazzei, A. *Inorg. Chim. Acta* **1973**, *7*, 319–322. (d) Marks, T. J.; Seyam, A. M.; Kolb, J. R. *J. Am. Chem. Soc.* **1973**, *95*, 5529–5539. (e) Cernia, E.; Mazzei, A. *Inorg. Chim. Acta* **1974**, *10*, 239–252. (f) Marks, T. J.; Kolb, J. R. *J. Am. Chem. Soc.* **1975**, *97*, 27–33. (g) Bagnall, K. W.; Plews, M. J.; Brown, D.; Fischer, R. D.; Klähne, E.; Landgraf, G. W.; Sienel, G. R. *J. Chem. Soc., Dalton Trans.* **1982**, 1999–2007. (h) Ossola, F.; Rossetto, G.; Zanella, P.; Paolucci, G.; Fischer, R. D. *J. Organomet. Chem.* **1986**, *309*, 55–63.

(13) (a) Averill, F. W.; Ellis, D. E. *J. Chem. Phys.* **1973**, *59*, 6411–6418. (b) Rosen, A.; Ellis, D. E.; Adachi, H.; Averill, F. W. *J. Chem. Phys.* **1976**, *65*, 3629–3634 and references therein. (c) Trogler, W. C.; Ellis, D. E.; Berkowitz, J. *J. Am. Chem. Soc.* **1979**, *101*, 5896–5901. (d) Ellis, D. E. In *Actinides in Perspective*; Edelstein, N. M., Ed.; Pergamon Press: Oxford, U.K., 1982; pp 123–143. (e) Delley, B.; Ellis, D. E. *J. Chem. Phys.* **1982**, *76*, 1949. (f) Gulino, A.; Casarin, M.; Conticello, V. P.; Gaudiello, J. G.; Mauermann, H.; Fragalà, I.; Marks, T. J. *Organometallics* **1988**, *7*, 2360–2364. (g) Casarin, M.; Ciliberto, E.; Gulino, A.; Fragalà, I. *Organometallics* **1989**, *8*, 900–906.

(14) Casarin, M.; Vittadini, A.; Granozzi, G.; Fragalà, I.; Di Bella, S. *Chem. Phys. Lett.* **1987**, *141*, 193–197.

Table I. Orbitals, Eigenvalues, and Population Analysis for $U(C_5H_5)_3^+$

MO	-GS,[a] eV	U 7s	U 7p	U 6d	U 5f	3Cp	character
$11a_1$	5.51	4	0	55	2	39	$d_{z^2} + \pi_3$
$6a_2$	7.75	0	0	0	61	39	$f_{y(3x^2-y^2)} + \pi_2$
15e	8.45	0	0	0	84	16	$f_{xyz} + f_{z(x^2-y^2)} + \pi_2$
$10a_1$	8.60	0	0	0	91	9	$f_{z^3} + f_{x(x^2-3y^2)}$
$9a_1$	8.63	0	0	0	97	3	$f_{x(x^2-3y^2)} + f_{z^3}$
14e	8.79	0	0	0	97	3	$f_{xz^2} + f_{yz^2}$ (HOMO)
$5a_2$	9.76	0	0	0	35	65	$\pi_2 + f_{y(3x^2-y^2)}$
13e	10.03	0	0	3	15	82	$\pi_2 + f_{z(x^2-y^2)} + f_{xyz}$
$8a_1$	10.12	0	0	2	8	90	$\pi_2 + f_{z^3}$
12e	10.57	0	0	8	0	92	$\pi_2 + d_{x^2-y^2} + d_{xy}$

[a] GS = ground state in all tables.

energies (IE's) were evaluated within the Slater transition-state formalism (TSIE's)[15] to account for reorganization effects upon ionization. Contour plots (CP's) of some selected molecular orbitals (MO's) have also been analyzed. The exchange parameter α was set to a uniform value of 0.7 in all calculations. Geometrical parameters used were taken from published X-ray data.[16] The model compound UCp_3NH_2 was employed for calculations on UCp_3NEt_2, and geometrical parameters were taken from data in ref 16b. In all calculations, the geometry of the UCp_3^+ cluster was fixed with a typical[17] 117° Cp(centroid)–U–Cp(centroid) angle and a typical[17] 2.54 Å U–Cp(centroid) distance.[17] Calculations were carried out on a Vax-11/750 minicomputer.

Results and Discussion

The large majority of known UCp_3L complexes have trigonally distorted pseudotetrahedral geometries[17] which usually contain a unique monodentate L^- ligand but are flexible enough to accommodate, despite the apparent steric congestion, even more coordinatively demanding ligands. In this class of complexes, including those presently studied, the UCp_3^+ fragment is a metrical constant feature and, hence, the related electronic structures can be better described in terms of perturbations induced by the bound L ligand upon the UCp_3 manifold.

Earlier electronic structure studies[5,8e,18] have shown that the η^5 hapticity of the Cp anion ligand mainly involves the 2-fold degenerate π_2 orbitals, the combinations of which, under the C_{3v} symmetry of the Cp_3 manifold, result in six orbitals:

$$3\text{-}\pi_2\ (e_1'' \text{ in } D_{5h}) \rightarrow a_1 + a_2 + e(1) + e(2)\ (\text{in } C_{3v})$$

These are spread over an ~1 eV energy range, and the sequence found in the present study

$$a_2 > e(2) > e(1) \approx a_1$$

reproduces results of these earlier calculations.[5,8e,18] It is noteworthy that, among these orbitals, the first two are destabilized relative to the energy baricenter of the unperturbed Cp-π_2 orbitals while the remaining lie lower. Simple, naive chemical intuition suggests that the stability of the MCp_3 cluster must, therefore, require ligand–metal donor interactions capable of stabilizing at least the a_2 and e(2) orbitals and, hence, of redistributing some ligand electron density onto the metal center.

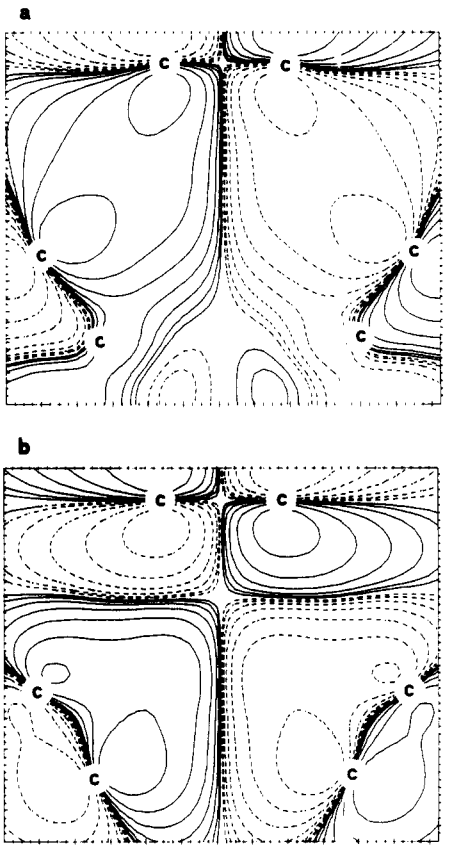

Figure 1. DV–Xα contour plots of the (a) 12e and (b) 13e MO's in the plane z = 2.5 au for the UCp_3^+ fragment. The contour values are ±0.0065, ±0.013, ±0.026, ±0.052, ±0.104, ±0.208, ±0.416, and ±0.832 $e^{1/2}$ Å$^{3/2}$. Dashed lines refer to negative values.

As a matter of fact, a significant metal–ligand covalency, and hence a large charge donation to the metal center, is associated in the UCp_3^+ fragment with interactions involving metal 5f orbitals. This is represented by the $5a_2$ MO (Table I). A minor contribution (8%) is also contributed by the $8a_1$ MO. Interestingly enough, the remaining π_2-related orbitals of e symmetry selectively interact with metal subshells because the shapes (Figure 1) of the 13e and 12e MO's selectively match those of the $5f_{z(x^2-y^2)}$ and of $6d_{xy}$ AO's, respectively. The total metal contribution to the MO's of the π_2 nest is 18% (5% 6d, 13% 5f) with a 82% ligand character. These values compare well (once the nonrelativistic nature of the present calculations is taken into account) with the 11% 6d and 11% 5f recently reported for UCp_3 using quasi-relativistic Xα–SW calculations.[8e] Furthermore, the metal 6d subshells are mostly admixed into the empty Cp π_3*-related MO's. In this context, the stabilization of the $11a_1$ MO (mostly $6d_{z^2}$ in nature), which lies lower than the orbitals of the π_3* nest[8f] (Figure 2) and is contiguous in energy with 5f subshells, is of particular relevance. This orbital is ideally suited to act as an acceptor orbital for coordination of the fourth L ligand.

$U(Cp)_3L$ Complexes. Population data for the present UCp_3L complexes (L = BH_4^-, $-CH_3$, $-NH_2$, $-NCS$) (Tables I–V) are similar and, of course reminiscent of those of

(15) Slater, J. C. *Quantum Theory of Molecules and Solids. The Self-Consistent Field for Molecules and Solids*; McGraw-Hill: New York, 1974.

(16) (a) Bernstein, E. R.; Hamilton, W. C.; Keiderling, T. A.; La Placa, S. J.; Lippard, S. J.; Mayerle, J. J. *Inorg. Chem.* **1972**, *11*, 3009–3016. (b) Perego, G.; Cesari, M.; Farina, F.; Lugli, G. *Gazz. Chim. Ital.* **1975**, *105*, 643–646. (c) Fischer, R. D.; Klähne, E.; Kopf, J. *Z. Naturforsch., B* **1978**, *33*, 1393–1397. (d) Rebizant, J.; Apostolidis, C.; Spirlet, M. R.; Kannellakopulos, B. *Inorg. Chim. Acta* **1987**, *139*, 209–210. (e) Cramer, R. E.; Engelhardt, U.; Higa, K. T.; Gilje, J. W. *Organometallics* **1987**, *6*, 41–45. (f) Cramer, R. E.; Edelmann, F.; Mori, A. L.; Roth, S.; Gilje, J. W.; Tatsumi, K.; Nakamura, A. *Organometallics* **1988**, *7*, 841–849.

(17) (a) Wong, C.; Yen, I.; Lee, T. *Acta Crystallogr.* **1965**, *10*, 430. (b) Ryan, R. R.; Penneman, R. A.; Kannellakopulos, E. *J. Am. Chem. Soc.* **1975**, *97*, 4258–4260. (c) Shannon, R. D. *Acta Crystallogr., Sect. A* **1976**, *A32*, 751–767. (d) Perego, G.; Cesari, M.; Farina, F.; Lugli, G. *Acta Crystallogr., Sect. B* **1976**, *B32*, 3034. (e) Raymond, K. N. In ref 1j, pp 249–280. (f) Raymond, K. N.; Eigenbrot, C. W., Jr. *Acc. Chem. Res.* **1980**, *13*, 276.

(18) (a) Evans, S.; Green, M. L. H.; Jewitt, A. F.; Orchard, A. F.; Pygall, C. F. *J. Chem. Soc., Faraday Trans. 2* **1972**, *68*, 1847–1865. (b) Evans, S.; Green, M. L. H.; Jewitt, A. F.; King, G. H.; Orchard, A. F. *J. Chem. Soc., Faraday Trans. 2* **1974**, *70*, 356–376.

Table II. Orbitals, Eigenvalues, Ionization Energies, and Population Analysis for the Uppermost $U(C_5H_5)_3BH_4$ MO's

				U						
MO	-GS, eV	TSIE,[a] eV	IE,[b] eV	7s	7p	6d	5f	3Cp	BH_4	character[c]
15e	4.47	6.83	6.93 (x)	0	1	1	94	3	2	$f_{xyz} + f_{z(x^2-y^2)}$
$5a_2$	5.88	8.00	8.04 (a)	0	0	0	24	76	0	$\pi_2 + f_{y(3x^2-y^2)}$
14e	5.99	8.08	8.45 (b)	0	0	1	19	73	7	$\pi_2 + f_{xz^2} + f_{yz^2}$
$10a_1$	6.37	8.45	8.76 (c)	0	0	2	5	91	2	π_2
13e	6.66	8.76	9.25 (d)	0	0	4	1	92	3	π_2
12e	8.75	10.85	10.79 (e)	0	0	3	1	48	48	$B-H_b + \pi_i$
$9a_1$	7.92	11.02		0	0	2	1	3	94	$B-H_t$
11e	9.01	11.13		0	0	1	0	60	39	$\pi_i + B-H_b$

[a] TSIE = transition-state ionization energy in all tables. [b] See Figure 6. [c] $H_b = H_{bridging}$, $H_t = H_{terminal}$.

Table III. Orbitals, Eigenvalues, Ionization Energies, and Population Analysis for the Uppermost $U(C_5H_5)_3CH_3$ MO's[a]

				U						
MO	-GS, eV	TSIE, eV	IE,[b] eV	7s	7p	6d	5f	3Cp	CH_3	character
15e	4.21 (5.41)	6.60 (8.36)	6.56 (x)	0 (0)	0 (0)	0 (0)	96 (96)	4 (4)	0 (0)	$f_{xyz} + f_{z(x^2-y^2)}$
$10a_1$	5.10 (6.27)	7.41 (9.03)	7.74 (a)	0 (0)	0 (0)	4 (3)	13 (15)	26 (25)	57 (57)	$CH_3 + f_{z^3} + d_{z^2}$
$5a_2$	5.59 (6.95)	7.74 (9.39)		0 (0)	0 (0)	0 (0)	25 (22)	75 (78)	0 (0)	$\pi_2 + f_{y(3x^2-y^2)}$
14e	5.90 (7.21)	8.00 (9.83)	8.47 (b)	0 (0)	0 (0)	3 (2)	11 (11)	85 (86)	1 (1)	$\pi_2 + f_{z(x^2-y^2)} + f_{xyz} + f_{xz^2} + f_{yz^2}$
$9a_1$	6.25 (7.44)	8.34 (10.84)		0 (0)	0 (0)	7 (5)	8 (9)	71 (74)	14 (12)	$\pi_2 + d_{z^2} + f_{z^3}$
13e	6.45 (7.68)	8.56 (11.00)	9.01 (c)	0 (0)	0 (0)	6 (5)	0 (0)	93 (94)	1 (1)	$\pi_2 + d_{xy} + d_{x^2-y^2}$

[a] Values in parentheses refer to multipolar DV-Xα calculation. [b] See Figure 7.

Table IV. Orbitals, Eigenvalues, Ionization Energies, and Population Analysis for the Uppermost $U(C_5H_5)_3NH_2$ MO's

				U						
MO	-GS, eV	TSIE, eV	IE,[a] eV	7s	7p	6d	5f	3Cp	NH_2	character
20a″	3.90	6.35	6.22 (x)	0	0	0	96	4	0	f_{xyz}
24a′	5.06	7.42	7.44 (a)	0	0	0	28	17	55	$N_{2p} + f_{xz^2}$
19a″	5.28	7.43		0	0	2	25	75	0	$\pi_2 + f_{y(3x^2-y^2)}$
23a′	5.52	7.59	8.15 (b)	0	1	0	0	90	9	π_2
18a″	5.76	7.77		0	0	4	10	86	0	$\pi_2 + f_{yz^2} + f_{xyz}$
22a′	5.79	7.89		0	0	5	3	81	11	$\pi_2 + d_{xz} + d_{x^2-y^2} + f_{z(x^2-y^2)}$
17a″	6.18	8.29	8.90 (c)	0	0	8	0	92	0	$\pi_2 + d_{xy}$
21a′	6.28	8.38		0	0	10	0	81	9	$\pi_2 + d_{xz} + d_{x^2-y^2}$
20a′	7.50	10.28	9.84 (d)	0	0	12	6	7	75	$N_{2p} + d_{z^2} + f_{z^3}$

[a] See Figure 8.

Table V. Orbitals, Eigenvalues, Ionization Energies, and Population Analysis for the Uppermost $U(C_5H_5)_3NCS$ MO's

				U								
MO	-GS, eV	TSIE, eV	IE,[a] eV	7s	7p	6d	5f	3Cp	N	C	S	character
16e	4.48	6.74	6.95 (x)	0	0	0	94	4	1	0	1	$f_{xyz} + f_{z(x^2-y^2)}$
15e	5.36	7.75	8.11 (a)	0	0	0	12	4	25	0	59	$np(N,S) + f_{xz^2} + f_{yz^2}$
$5a_2$	5.84	7.85	8.33 (a′)	0	0	0	25	75	0	0	0	$\pi_2 + f_{y(3x^2-y^2)}$
$12a_1$	6.09	8.08	8.84 (b)	0	0	0	2	96	2	0	0	π_2
14e	6.15	8.13	9.09 (b′)	0	0	3	9	85	0	0	3	$\pi_2 + f$
13e	6.69	8.69	9.22 (c)	0	0	6	0	93	0	0	1	$\pi_2 + d$
12e	8.63	10.34	10.69 (d)	0	0	0	0	2	32	54	12	np(NCS)
11e	8.77	10.76		0	0	0	0	100	0	0	0	π_i
$11a_1$	9.17	11.28		0	0	4	1	27	49	1	18	$N_{2p} + d_{z^2}$

[a] See Figure 9.

analogous complexes, including the UCp_3^+ fragment.[5i,6,8e,f] It is important to note that results of multipolar DV-Xα calculations are identical with those of SCC runs so far as the derived energy sequences and atomic compositions are concerned. Of course, differences in GS and TSIE absolute energy values are found, even though SCC results provide a more accurate fitting of PE data[13e] (Table III). Therefore, SCC results only will be discussed hereafter. The upper filled MO's are grouped in well-defined energy ranges depending upon the dominant atomic contribution (Tables I–V). Thus, the metal subshell responsible for the uranium $5f^2$ configuration lies lowest, in the 6.35–6.83-eV range. Where allowed by symmetry (L = $-CH_3$, $-BH_4$, -NCS), the HOMO consists of a pair of degenerate orbitals of almost pure 5f character. Of course, the lower C_s symmetry of UCp_3NH_2 results in a singly degenerate 20a″ HOMO ($5f_{xyz}$ in nature) which, however, is almost degenerate (within a few tenths of an electronvolt) with the $f_{x(x^2-3y^2)}$ LUMO. Next and somewhat overlapped with the π_2-based MO's are additional orbitals ($10a_1$, 24a′, and 15e) which represent σ (L = CH_3) or π (L = $-NH_2$, -NCS) U-L bonds (Tables III–V). The nest of Cp π_2-related MO's follows in the 7.43–8.76-eV range with the same ordering which has proven ubiquitous[5i] in other MCp_3L complexes: $a_2 > e(2) > a_1 > e(1)$. The different sequence $a_1 > e(2)$ is found only in the cases of L = $-NH_2$ and -NCS. The inverted sequence[19] (Tables IV and V) depends upon interligand interactions with suitable MO's related to the σ M-L bond. Finally, the window between 9 and 11 eV is unique for each complex and includes, in terms of a localized bonding model, the U—N σ bond (L = $-NH_2$),

(19) Note that in UCp_3NH_2, the following symmetry correlations apply: $5a_2 \rightarrow 19a''$; $10a_1 \rightarrow 23a'$; $13e \rightarrow 18a'' + 22a'$; $12e \rightarrow 17a'' + 21a'$.

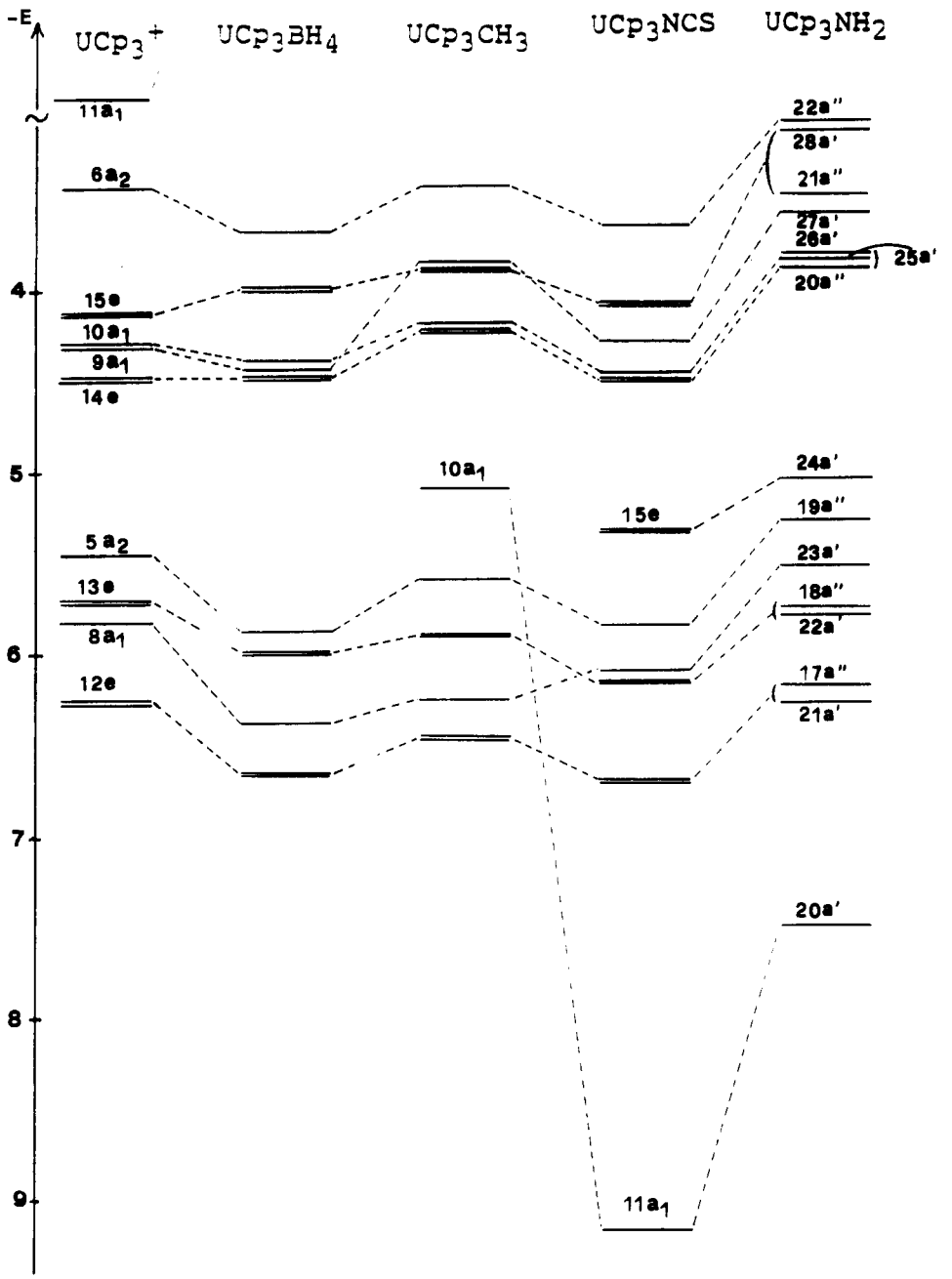

Figure 2. Correlation diagram between the ground-state eigenvalues of UCp_3^+, UCp_3BH_4, UCp_3CH_3, UCp_3NCS, and UCp_3NH_2. The Cp_3U^+ levels have been shifted (5.3 eV) to higher energy.

the B—H bonds (L = $-BH_4$), and the N=C π bond (L = –NCS). The innermost Cp-π_1 and other σ orbitals are beyond 10.30–12 eV and are not reported in the tables.

In the UCp_3BH_4 complex, the tetrahydroborate anion acts as a tridentate ligand through bridging hydrogens.[12f,16a] The Xα population data (Table II) provide an indication that the bridging of the BH_4^- anion results in only a minor perturbation of the UCp_3^+ fragment. However, there is evidence of an unusual interligand nonbonded interaction involving the innermost Cp-π_1 and bridging U–H–B orbitals (12e, 11e[20] MO's). The U–H_b related overlap population values (Table VI) are consistent with these data. The η^3 bridging of the $-BH_4$ ligand mostly involves metal 6d orbitals (12e in Table II), but given the small metal contribution, the bonding appears highly electrostatic in character, in accordance with literature data.[11]

Interactions with the $-CH_3$ ligand appear to be σ-only in nature (Table III) and are comparably contained in the $10a_1$ and $9a_1$ MO's. The metal 6d contribution in the latter is significantly higher than that found in UCp_3^+ (7% vs 2%), due to the intermediacy of an interligand admixture which expands the corresponding wave function toward the U–C(CH_3) region, thus favoring interaction with the metal $6d_{z^2}$ orbital. The related contour plots for both orbitals (Figure 3) show a rather substantial accumulation of σ electron density in the U–C(CH_3) region because of donation of the σ methide lone pair into the axially oriented $12a_1$ and $15a_1$,[21] empty acceptor orbitals that are $5f_{z^3}$- and $6d_{z^2}$-based, respectively.

The L = $-NH_2$ ligand is, of course, isoelectronic with the aforementioned ligands. However, it possesses a filled N_{2p} lone pair suitable for π-bonding. The U–N bond is for-

(20) The 11e MO lies, at –9.01 eV, out of the energy range reported in Table I.

(21) The $15a_1$ empty MO lies at 3.54 eV, out of the energy range of Table I.

Table VI. Electronic Charge and Overlap Population for UCp_3L Complexes

	charge						
	U						
complex	5f	6d	7s	7p	Cp	L	overlap population
UCp_3^+	3.465	0.696	0.020	0.048	−0.257	−1	U---Cp = 0.119
UCp_3NH_2	3.385	0.732	0.025	0.058	−0.514	−0.258	U---Cp = 0.104 U---NH_2 = 0.69
UCp_3CH_3[a]	3.392 (3.437)	0.709 (1.048)	0.023 (−0.088)	0.047 (−0.353)	−0.487 (−0.556)	−0.369 (−0.288)	U---Cp = 0.164 U---CH_3 = 0.392
UCp_3NCS	3.422	0.651	0.020	0.047	−0.454	−0.497	U---Cp = 0.166 U---N = 0.465 N---C = 1.544 C---S = 0.991
UCp_3BH_4	3.412	0.663	0.016	0.048	−0.386	−0.702	U---Cp = 0.167 U---BH_4 = 0.078 U---H_b = 0.0
UCp_3OCH_3[b]			+1.815		−0.518	−0.261	U---Cp = 0.050 U---OCH_3 = 0.709
UCp_3F[c]			+1.842		−0.490	−0.372	U---Cp = 0.0 U---F = 0.422
UCp_3Cl[c]			+1.818		−0.479	−0.381	U---Cp = 0.0 U---Cl = 0.433
UCp_3Br[c]			+1.801		−0.487	−0.340	U---Cp = 0.0 U---Br = 0.419

[a] Values in parentheses refer to a multipolar DV-Xα calculation. The negative population of diffuse 7s and 7p uranium components is due to the charge density casting in a multicenter overlapping multipolar form. See: Ellis, D. E.; Berkovitch-Yellin, Z. *J. Chem. Phys.* **1981**, *74*, 2427–2435. See also: Casarin, et al. *Chem. Phys. Lett.* **1987**, *141*, 193–197. [b] Taken from ref 10c. [c] Gulino, A.; Fragalà, I., unpublished results.

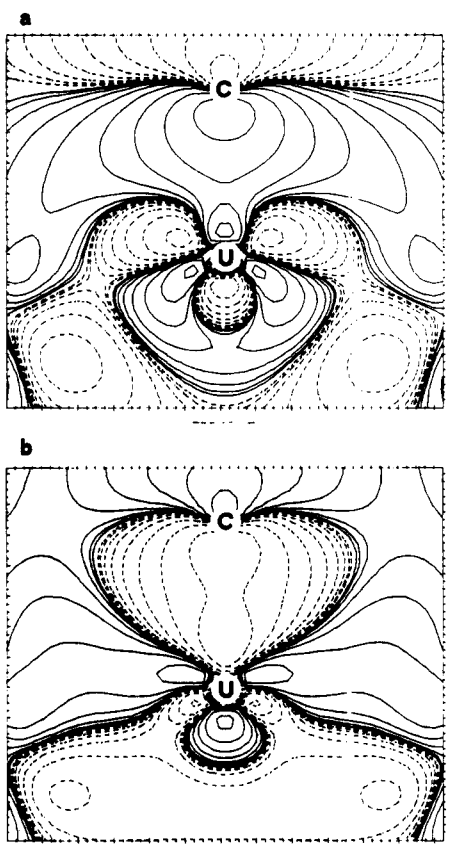

Figure 3. DV-Xα contour plots of the (a) $10a_1$ and (b) $9a_1$ MO's in the *yz* plane for the UCp_3CH_3 molecule. The contour values are ±0.0065, ±0.013, ±0.026, ±0.052, ±0.104, ±0.208, ±0.416, and ±0.832 $e^{1/2}$ Å$^{3/2}$. Dashed lines refer to negative values.

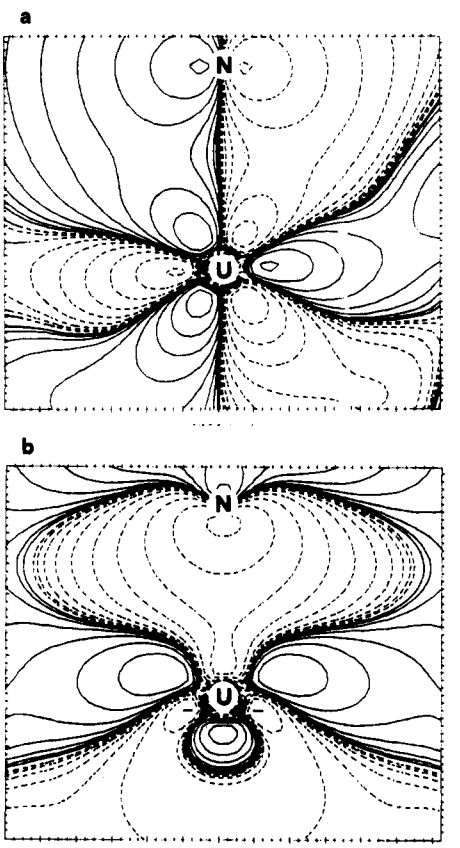

Figure 4. DV-Xα contour plots of the (a) 24a′ and (b) 20a′ MO's in the *xz* and *yz* planes, respectively, for the UCp_3NH_2 molecule. The contour values are ±0.0065, ±0.013, ±0.026, ±0.052, ±0.104, ±0.208, ±0.416, and ±0.832 $e^{1/2}$ Å$^{3/2}$. Dashed lines refer to negative values.

mally represented by the 24a′ and 20a′ MO's (Table IV). The 24a′ orbital (SHOMO) has a π symmetry along the U–N internuclear axis (Figure 4) and involves the N_{2p} lone pair and the metal $5f_{xz^2}$ AO. It possesses some Cp admixture due to interaction with the 22a′ MO. The 20a′ MO represents the σ U–N bond (Figure 4), which mostly consists of an admixture of the N_{2p} σ lone pair and the $6d_{z^2}$ metal orbital (12%).

X-ray data[16c] have shown that coordination of the NCS^- anion to UCp_3^+ results in the formation of a U—N bond and a linear U—N=C=S framework. A close analogy exists between NCS^- and the linear, isoelectronic carbon dioxide molecule, which is instructive in understanding UCp_3^+–NCS^- bonding. Thus, the electronic structure of CO_2 has been discussed in terms of the topmost filled $1\pi_g$,

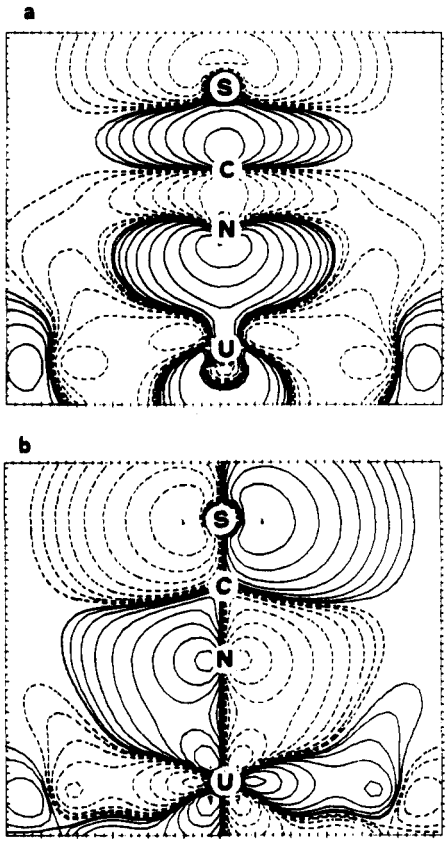

Figure 5. DV-Xα contour plots of the (a) $11a_1$ and (b) 15e MO's in the *yz* plane for the UCp_3NCS molecule. The contour values are ±0.0065, ±0.013, ±0.026, ±0.052, ±0.104, ±0.208, ±0.416, and ±0.832 $e^{1/2}$ $Å^{3/2}$. Dashed lines refer to negative values.

$1\pi_u$, $3\sigma_u^+$, and $4\sigma_g^+$ MO's.[22] Population data (Table V) and a contour plot analysis of the 15e, 12e, and $11a_1$ MO's of $UCp_3(NCS)$ show them to be topologically close counterparts of the uppermost three MO's of CO_2. In particular, the NCS^- 12e orbital is almost unaffected by the UCp_3^+ coordination and, therefore, represents the uppermost orbital of the –NCS π system. In contrast, the 15e and $11a_1$ MO's are admixed with the $5f_{xz^2}$, $5f_{yz^2}$, and $6d_{z^2}$ metal orbitals, thus contributing to U–N π and σ bonds, respectively (Figure 5). This observation finds a close counterpart in the description of the U–N bonding found in UCp_3NH_2 (vide supra). The π_2-related MO's remain almost totally unaffected by the –NCS coordination (Table V).

Photoelectron Spectra. Despite the neglect of relativistic effects, the theoretical Xα data accurately reproduce the experimental PE IE's as well as the observed He I/He II relative intensity changes. Relative partial photoionization cross-sections to be used as references for metal-5f organometallics[7] have been recently and accurately determined using synchrotron radiation.[7] At the He II wavelength, 5f ionizations show a "delayed maximum" in accordance with earlier results.[7] Consequently, ligand-based orbitals having some metal 5f contributions show a slower (than those metal 6d admixed) falloff in the cross-section in the 20–40-eV photon range as a consequence of the aforementioned maximum.

The present PE spectra all show lower intensity onset features (labeled **x** in the figures) which have proven to be ubiquitous in the spectra of all the U(IV) complexes studied to date. This band is absent in the corresponding Th(IV) complexes[23] and undergoes the usual relative intensity enhancement[5] in the He II spectra. The **x** band, therefore, can be confidently associated with production of the $^2F_{5/2}$ state upon ionization from the $^3H_4$ ground state of the U(IV) $5f^2$ configuration. As usual, there is no evidence of the $J = {}^7/_2$ state or of any additional structure due to crystal field effects.[4a,24]

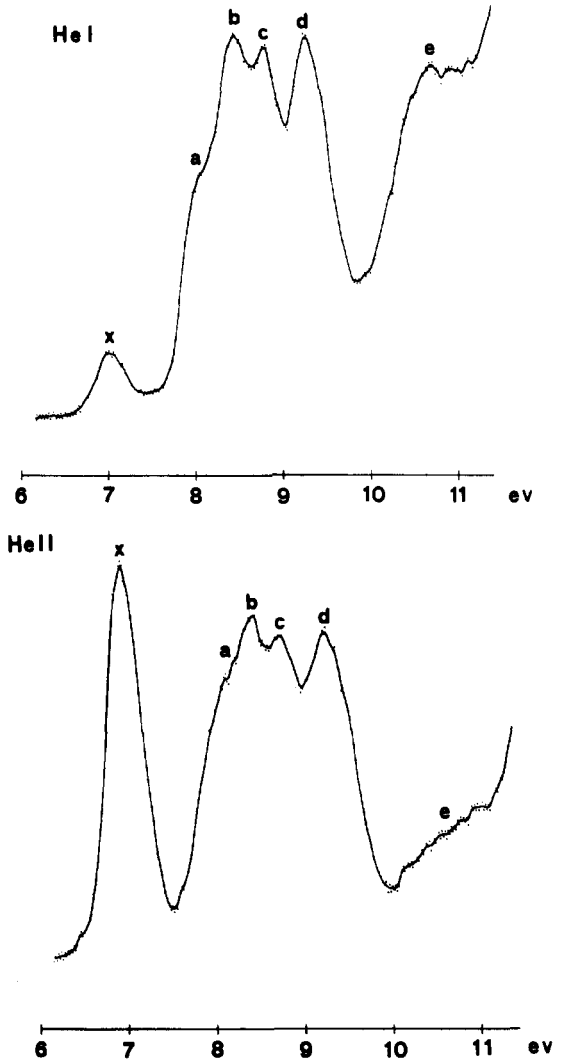

Figure 6. He I and He II PE spectra of UCp_3BH_4 (6–11.4 eV).

The spectrum of the L = $-BH_4$ complex shows four resolved structures in the 7.6–9.8-eV region (Figure 6) which must be assigned (Table II) to π_2-related MO's, since no ionizations due to the $-BH_4$ ligand are expected in this region.[5j,25] Next, band d is taken to represent ionizations of the 12e and $9a_1$ ($-BH_4$-based) MO's in accordance with TSIE values (Table II) and earlier PE data.[5j,25] In the He II spectrum, feature a increases in relative intensity due to the calculated ~24% 5f contribution to the corresponding $5a_2$ MO, while band d appears consistently smaller, as found with other closely related U(IV) organometallics.[5j,25] Notably, UCp_3BH_4 represents the first case among UCp_3L complexes in which individual π_2-related MO's are identified in well-resolved PE spectral features.

In the spectra of the L = $-CH_3$ and $-NH_2$ complexes (Figures 7 and 8), the bands between ca. 7 and 9.5 eV are

(22) Eland, J. H. D. *Philos. Trans. R. Soc. London, A* **1970**, *287*, 87–96.

(23) Gulino, A.; Fragalà, I., research in progress.

(24) (a) McLaughlin, R. *J. Chem. Phys.* **1962**, *36*, 2699. (b) Egdelll, R. G. Ph.D. Thesis, Oxford University, 1977.

(25) (a) Green, J. C.; Shinomoto, R.; Edelstein, N. *Inorg. Chem.* **1986**, *25*, 2718–2720. (b) Down, A. J.; Egdell, R. G.; Orchard, A. F.; Thomas, P. D. P. *J. Chem. Soc., Faraday Trans. 2* **1978**, 1755.

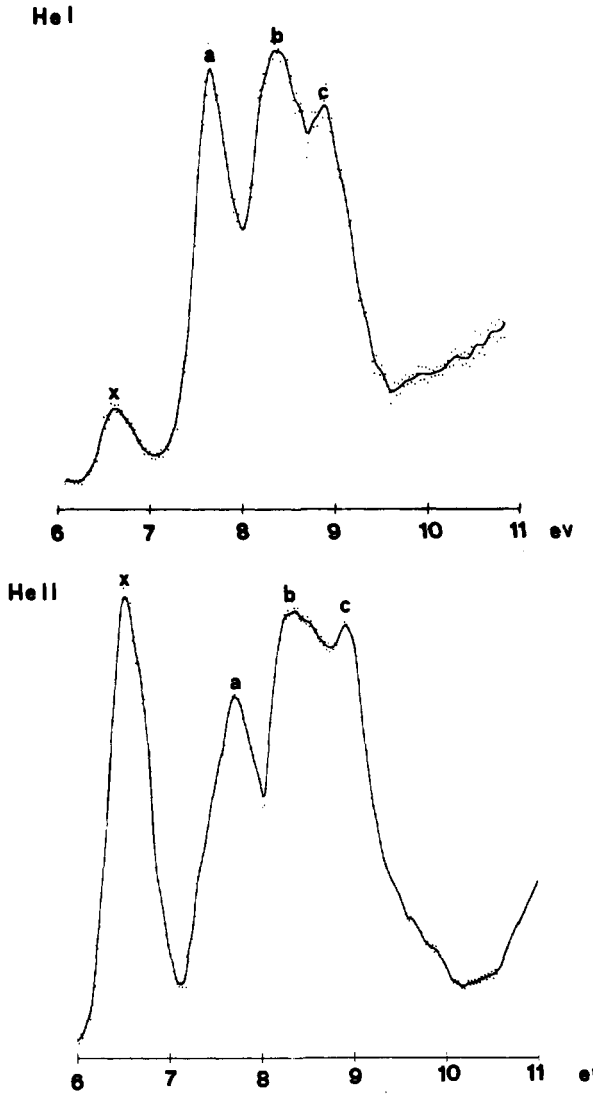

Figure 7. He I and He II PE spectra of UCp_3CH_3 (6–11 eV).

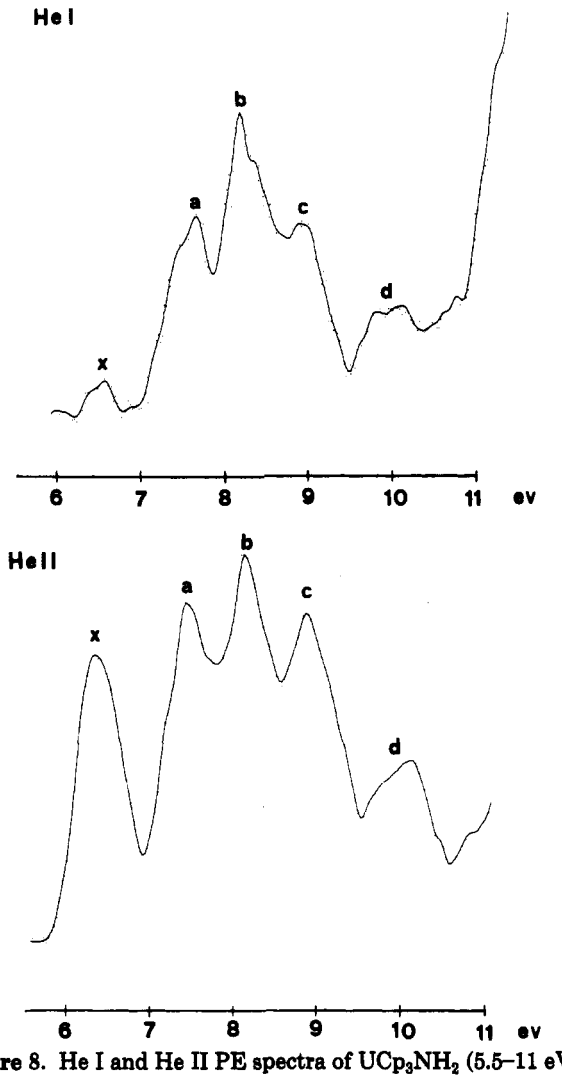

Figure 8. He I and He II PE spectra of UCp_3NH_2 (5.5–11 eV).

closely reminiscent of the "classical" triplet structure found in several other MCp_3L (L = F, Cl, Br) complexes[3b,5a,h] and are assigned to ionization of π_2-related Cp MO's. The intensity branching ratios between the three main components differ, however, from the usual[3b,5a,i] 1:3:2 values. In the case of UCp_3CH_3, a roughly 2:3:2 ratio is observed. Band a, in fact, includes, in addition to the $(5a_2)^{-1}$ and $(10a_1)^{-1}$ ionization in accordance with both present calculations and earlier PE data for various d- and f-element methyl complexes.[5c,26] The bands up to 10 eV are straightforwardly associated with the remaining π_2-related MO's (Table III). Under He II radiation, bands a and b become less intense relative to c. Although some underestimation of the 6d contribution to the π_2-related MO's must be expected (vide supra), the combined behavior of bands a and c remains open to question since the 5f contribution to the a_2 MO is constrained by symmetry, while there is no doubt about the metal-6d-only contribution to the 13e MO (Table III). Nevertheless, an unexpected He II enhancement of PE bands representing more internal Cp-π_2 orbitals has been observed in the PE spectra of other Cp complexes,[5h] while limitations due to the Gelius model[27] approximation generally adopted to interpret PE data might be more apparent in the present case.

In the case of the L = $-NH_2$ complex, a nearly 2:3:2 ratio is observed in the 7–9.5-eV region (Figure 8). Band a represents the $(24a')^{-1}$ and $(19a'')^{-1}$ ionizations. Its relative intensity increases on passing to He II radiation, in accordance with the very large metal 5f character of the 24a′ and 19a″ MO's (Table IV). Bands b and c are assigned according to TSIE values (Table IV) and, in analogy to other UCp_3L complexes,[3b,5a,i] to ionizations of π_2-related MO's. Similar to both $UCp_2(NR_2)_2$ and other amido complexes,[5j,28] there is evidence, between 9 and 10 eV, of an additional band (d) which represents (Table IV) ionization of the 20a′ MO, whose intensity in the He II spectrum is in excellent agreement with dominant metal 6d orbital contributions.

Finally, the spectrum of UCp_3NCS (Figure 9) consists, in the 7.5–10-eV region, of a simple doublet structure with an approximately 3:5 intensity ratio. The two main components are partially structured into two and three components, respectively. TSIE values (Table V) suggest the

(26) (a) Evans, S.; Green, J. C.; Joachim, P. J.; Orchard, A. F.; Turner, D. W.; Maier, J. P. *J. Chem. Soc., Faraday Trans 2* **1972**, *68*, 905–911. (b) Lappert, M. F.; Pedley, J. B.; Sharp, G. *J. Organomet. Chem.* **1974**, *66*, 271–278. (c) Barker, G. K.; Lappert, M. L.; Pedley, J. B.; Sharp, G. J.; Westwood, N. P. C. *J. Chem. Soc., Dalton Trans.* **1975**, 1765. (d) Creber, D. K.; Bancroft, G. M. *Inorg. Chem.* **1980**, *19*, 643–648. (e) Bruno, G.; Ciliberto, E.; Di Bella, S.; Fragalà, I.; Müller, G. *Organometallics* **1990**, *9*, 1629–1643.

(27) Gelius, U.; Siegbahn, K. *Faraday Discuss. Chem. Soc.* **1972**, *54*, 257.

(28) (a) Gibbins, S. G.; Lappert, M. F.; Sharp, G. J. *J. Chem. Soc., Dalton Trans.* **1975**, 72–76. (b) Lappert, M. F.; Pedley, J. B.; Sharp, G. J.; Brandley, D. C. *J. Chem. Soc., Dalton Trans.* **1976**, 1737–1740. (c) Harris, D. H.; Lappert, M. F.; Pedley, J. B.; Sharp, G. J. *J. Chem. Soc., Dalton Trans.* **1976**, 945–950.

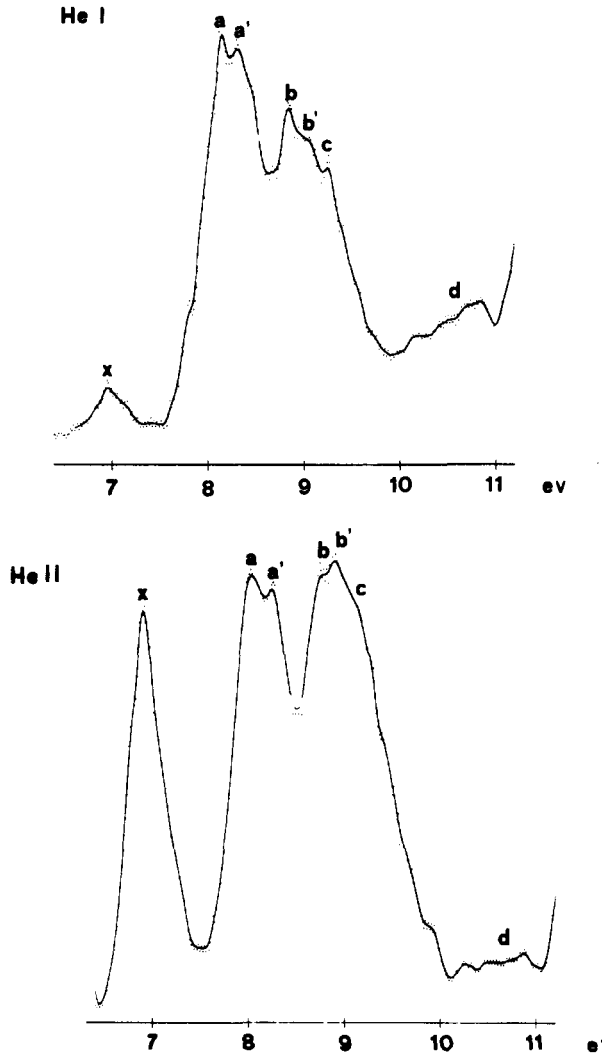

Figure 9. He I and He II PE spectra of UCp_3NCS (6.2–11.2 eV).

assignment of structures a and a′ to ionizations of the 15e and $5a_2$ MO's, respectively. The reduced relative intensity of envelope a under He II radiation is in good agreement with the 59% S_{3p} contribution to the 15e MO and, in turn, with the well-known falloff of the He II S_{3p} cross-section.[29] The remaining band envelopes b, b′, and c are assigned to ionizations of the $12a_1$, 14e, and 13e MO's. In the window between 10 and 11 eV there is evidence of a poorly resolved structure which certainly includes the $(12e)^{-1}$ ionization, since the reduced He II relative intensity agrees well with the S_{3p} admixture into the corresponding MO.

Conclusions

The electronic structure of a series of UCp_3L complexes has been investigated as a function of L using the SCF Hartree–Fock–Slater first-principles discrete variational Xα approach, thus revealing interesting details of the metal–ligand bonding. The Cp_3^{3-} ligand cluster uses π_2-related MO's for bonding interactions involving both metal 5f and 6d orbitals. Symmetry properties render the $5f_{y(3x^2-y^2)}$ AO unique for stabilizing ligand MO's of a_2 symmetry and thus render 5f elements excellent templates for coordination of the Cp_3^{3-} cluster. Interactions not restricted by symmetry appear partially or entirely modulated by the angular properties of π_2-related MO's. However, the bonding interactions with the L ligands are more diverse. These interactions preferentially involve either $5f_{z^3}$ or $6d_{z^2}$ metal orbitals, depending upon the energies of the unperturbed ligand orbital counterparts. Hence, the more internal σ(–NH_2) and σ(–NCS) bonding orbitals mostly mix with metal 6d orbitals, while the more external σ(–CH_3), π(–NH_2), and π(–NCS) bonding orbitals mostly interact with metal 5f orbitals. Therefore, the M–L bonding appears to be largely ionic in nature for L = BH_4^-, σ-only in character for L = –CH_3, and σ with some π character for L = –NCS. Finally, the –NH_2 ligand, in addition to the classical σ M–L bond, uses the N_{2p} lone pair to form a π bond.

The energies of U 5f orbitals, including the HOMO's (Tables I–V), are similarly distributed in all of the present complexes. The nonbonding $f_{ml} = \pm 1$ HOMO as well as the slightly antibonding $f_{ml} = \pm 2$ orbitals lie within a narrow (≤0.40 eV) range. Also observed is a remarkable "ligand field" energy shift (~0.8 eV) associated only with the $5f_{y(3x^2-y^2)}$ ($6a_2$) orbital (Figure 2), as a consequence of the considerable admixture (30%) with the Cp-based MO's.

The overall result of L→M charge donation is an almost constant configuration on the uranium atom and, hence, a comparable +1.8 ± 0.06 metal charge, despite the rather different nature of the σ-bonded L ligands (Tables I–VI). Interestingly enough, the metal electronic configuration remains almost constant along the series and similar to that ($5f^{3.4}$, $6d^{0.7}$) found in fully relativistic SCF Dirac–Slater calculations on the simpler uranium atom.[10a,c] This result illustrates a ligand→metal charge donation mechanism which maintains the energetically preferred configuration at the metal center.

It is also found that donation from the L ligand depends upon both the M–L covalency and the nature (σ and/or π) of the bonding. Therefore, more covalently bound L ligands have lower total charges as well as lower U 5f populations and U–Cp overlap values associated with them. Conversely, higher values are found for both 6d population and Cp charge values. It is seen that the stringent necessity of maintaining the uranium center in a particularly stable electronic configuration causes the larger donation (hence greater covalency in the bonding) from L ligands to be compensated for by an increasing (L = –NH_2 < –CH_3 < –NCS < –BH_4) ionic character of the U–Cp bonds. Inspection of population data reported in Table VI suggests that this effect does not involve a back-bonding mechanism. Rather, the metal subshells, when more extensively tied up in the U–L bonding, become less available for U–Cp interactions. We note in passing that the observed trend (Table VI) of the charge being localized over the entire Cp ligand set agrees well with the ^1H NMR (Cp) values.[11] Literature data show that higher field shifts are measured for those L ligands which are not only σ bonded but, in addition, possess π-donor capabilities.[11]

A final consideration concerns the use of the Xα–DV approach, even at a nonrelativistic level, combined with PE data to describe electronic structures of a closely related series of 5f complexes. The present data, as well as previous reports, have shown that nonrelativistic DV–Xα calculations, optimized in order to find the best basis set and potential representation,[4c] are well-suited counterparts to the PE data, including the He I/He II relative intensity changes, which in turn provide an experimental test of the theoretical description. It has been noted (vide supra) that neglecting relativistic operators underestimates to some degree the influence of 6d metal orbitals on metal–ligand covalency, which in turn is better described in relativistic

(29) Rabelais, J. W. *Principles of UV Photoelectron Spectroscopy*; Wiley: New York, 1977.

calculations. Nevertheless, even though relativistic results may better approach a quantitative description of the electronic structure, it is presently unclear whether such demanding computational efforts are worthwhile. In the case of far simpler molecules, such calculations improve the interpretation of PE data to only a limited extent. The matter, however, still remains open to question, and further studies will be reported in a forthcoming paper.[10c]

Acknowledgment. We gratefully thank the Ministero della Pubblica Istruzione (MPI, Rome, Italy; A.G., E.C., and I.F.) and the U.S. National Science Foundation (Grant CHE 9104112; A.M.S. and T.J.M.) for financial support.

Registry No. $U(\eta^5\text{-}C_5H_5)_3CH_3$, 37205-28-0; $U(\eta^5\text{-}C_5H_5)_3NH_2$, 112196-34-6; $U(\eta^5\text{-}C_5H_5)_3BH_4$, 37298-62-7; $U(\eta^5\text{-}C_5H_5)_3NCS$, 69526-48-3.

Supplementary Material Available: Orbitals, eigenvalues, and population analysis of Cp_3ThOCH_3 in C_s symmetry (Table SI) and in C_{3v} symmetry (Table SII) and relativistic orbitals, eigenvalues, and population analysis of Cp_3ThOCH_3 in C_{3v} symmetry (Table SIII) (2 pages). Ordering information is given on any current masthead page.

OM9202229

^{19}F NMR Studies of the Reaction of Octaphenylcyclotetrasilane with Triflic Acid

Jerzy Chrusciel, Marek Cypryk, Eric Fossum, and Krzysztof Matyjaszewski*

Department of Chemistry, Carnegie Mellon University, 4400 Fifth Avenue, Pittsburgh, Pennsylvania 15213

Received January 15, 1992

The chemo- and stereoselectivity of the dearylation reaction of octaphenylcyclotetrasilane with trifluoromethanesulfonic acid was studied using ^{19}F NMR. Up to four triflate groups could be easily introduced to the ring. Substitution of the fifth phenyl group was accompanied by ring cleavage. Dearylation competes with the exchange of silyl triflates with triflic acid and leads to the thermodynamic distribution of stereoisomers.

Introduction

Arylsilanes are known to undergo electrophilic displacement of aryl groups by strong protonic acids.[1-3] The first step of the reaction involves a reversible protonation of the ipso-carbon atom, followed by nucleophilic attack of the resulting anion on the silicon atom with cleavage of the C_{Ar}–Si bond.[1] Although this reaction is often referred to as *protodesilylation* in organic chemistry literature, we prefer the "silicocentric" term, *dearylation*, which is more suitable to discussions of reactions on the silicon backbone.

Labile functional groups such as halogens and perchlorate can be introduced onto silicon by silane dearylation, thus enabling further modification by a variety of nucleophilic reagents.[4-6] For example, functional silanes react with $LiAlH_4$, organometallic reagents, alcohols, and primary or secondary amines yielding silicon hydrides and organo-, alkoxy-, and aminosilanes, respectively.

Trifluoromethanesulfonic (triflic) acid is a versatile and very efficient dearylating reagent.[6,7] The resulting silyl triflates are among the most reactive silylating agents.[5,6] They also initiate the cationic polymerization of some vinyl and heterocyclic monomers[8] and can be converted to silyl ketene acetals for initiation of group transfer polymerization.[9] Thus, poly(tetrahydrofuran) and poly(methyl methacrylate) have been grafted onto poly(methylphenylsilylene) backbones which were dearylated with triflic acid.[9-11]

Scheme I

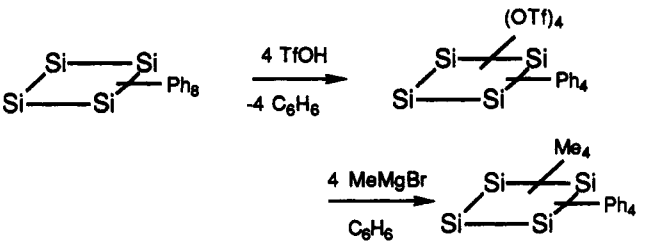

The kinetics of dearylation of dimethyldiphenylsilane[6] and α,ω-diphenylpermethyloligosilanes[12] have been studied. Although substitution of the first phenyl group is very fast, substitution of the second phenyl group in dimethyldiphenylsilane is several orders of magnitude slower due to deactivation by the electron-withdrawing triflate group. The reaction rate is 23 times lower when the TfO group is bound to the α Si atom in a disilane. Although this effect decreases with increasing separation of the phenyl and triflate groups, it is still significant at distances up to four Si–Si bonds. For example dearylation of the first Ph group in 1,5-diphenyldecamethylpentasilane is 7 times faster than dearylation of the second one.[12]

The replacement of aryl by alkyl groups in cyclotetrasilanes provides a route for the synthesis of strained rings such as 1,2,3,4-tetramethyl-1,2,3,4-tetraphenylcyclotetra-

(1) Eaborn, C. *J. Organomet. Chem.* **1975**, *100*, 43.
(2) Hengge, E.; Marketz, H. *Monatsh. Chem.* **1969**, *100*, 890.
(3) Hengge, E.; Kovar, D. *Angew. Chem., Int. Ed. Engl.* **1981**, *20*, 678.
(4) Hengge, E.; Marketz, H. *Monatsh. Chem.* **1970**, *101*, 528.
(5) Emde, H.; Domsch, D.; Feger, H.; Frick, U.; Gotz, A.; Hergott, H. H.; Hoffmann, K.; Kober, W.; Krageloh, K.; Oesterle, T.; Steppan, W.; West, W.; Simchen, G. *Synthesis* **1982**, 1.
(6) Matyjaszewski, K.; Chen, Y. L. *J. Organomet. Chem.* **1988**, *340*, 7.
(7) Habich, D.; Effenberger, F. *Synthesis* **1978**, 755.
(8) Gong, M. S.; Hall, H. K., Jr. *Macromolecules* **1986**, *19*, 3011.
(9) Hrkach, J.; Ruehl, K.; Matyjaszewski, K. *Polym. Prepr., Am. Chem. Soc. Div. Polym. Chem.* **1988**, *29* (2), 112.
(10) Matyjaszewski, K.; Hrkach, J.; Kim, H. K.; Ruehl, K. In *Silicon-Based Polymer Science*; Zeigler, J. M., Gorgon Fearon, F. W., Eds.; Advances in Chemistry Series 224; American Chemical Society: Washington, DC, 1990; p 285.
(11) Uhlig, W. *J. Organomet. Chem.* **1991**, *402*, C45.
(12) Ruehl, K.; Matyjaszewski, K. *J. Organomet. Chem.* **1991**, *410*, 1.

0276-7333/92/2311-3257$03.00/0